Copepod carcasses in the Subtropical Convergence Zone of the Sargasso Sea: Implications for microbial community composition, system respiration and carbon flux

Kam W. Tang[1*], Liv Backhaus[2], Lasse Riemann[2], Marja Koski[3], Hans-Peter Grossart[4,5], Peter Munk[3], Torkel Gissel Nielsen[3]

1. Department of Biosciences, Swansea University, Singleton Park, Swansea, SA2 8PP, U.K.
2. Department of Biology, University of Copenhagen, Strandpromenaden 5, 3000 Helsingør, Denmark
3. National Institute of Aquatic Resources, Technical University of Denmark, Kemitorvet, Building 202, 2800 Kgs. Lyngby. Denmark
4. Leibniz-Institute of Freshwater Ecology and Inlandwater Fisheries, Dept. Experimental Limnology, Alte Fischerhuette 2, D-16775 Stechlin, Germany
5. Potsdam University, Inst. Biochemistry and Biology, Maulbeerallee 2, D-14469 Potsdam, Germany

***Corresponding author:** k.w.tang@swansea.ac.uk

Keywords: Sargasso Sea; subtropical convergence zone; zooplankton; carcasses; carbon sinking flux

Abstract

The oligotrophic subtropical gyre covers a vast area of the Atlantic Ocean. Decades of time-series monitoring have generated detailed temporal information about zooplankton species and abundances at fixed locations within the gyre, but their live/dead status is often omitted, especially in the dynamic Subtropical Convergence Zone (STCZ) where the water column stratification pattern can change considerably across the front as warm and cold water masses converge. We conducted a detailed survey in the North Atlantic STCZ, and showed that over 85% of the copepods were typically concentrated in the upper 200 m. Copepod carcasses were present in all samples and their proportional numerical abundances increased with depth, reaching up to 91% at 300–400 m. Overall, 14–19% of the copepods within the upper 200 m were carcasses. Shipboard experiments showed that during carcass decomposition, microbial respiration increased, and the bacterial community associated with the carcasses diverged from that in the ambient water. Combining field and experimental data, we estimated that decomposing copepod carcasses constitute a negligible oxygen sink in the STCZ, but sinking carcasses may represent an overlooked portion of the passive carbon sinking flux, and should be incorporated in future studies of carbon flux in this area.

INTRODUCTION

About one-third of the world's ocean is classified as oligotrophic with low productivity and nutrient concentrations (Carr et al., 2006), much of which is located in the subtropical gyres. Given the vast area covered by the oligotrophic ocean, its biota and related ecological processes have far-reaching ramifications for global biogeochemical cycles and O_2/CO_2 balance (Ducklow and Doney, 2013). Based on multi-year SeaWiFS ocean color data, oligotrophic subtropical gyres appear to be expanding, and most rapidly in the North Atlantic (Polovina et al., 2008). As such, detailed understanding of the pelagic food web in these regions becomes increasingly important.

A considerable amount of research effort has been focused on these large marine ecosystems, as exemplified by long-running oceanographic time-series programs in the Sargasso Sea (BATS: Michaels and Knap, 1996; Steinberg et al., 2001) and near Hawaii (HOT: Karl and Lukas, 1996). While these time-series studies provide detailed temporal information of fixed locations, they do not capture the spatial variabilities across the gyres, especially in the subtropical convergence zone (STCZ) where the convergence of warm and cold waters creates complex frontal structures. Detailed biological data of the North Atlantic STCZ are limited (Böttger, 1982), although some studies have suggested that it is a key spawning and nursery ground for eel, presumably due to localized enhanced biological productivity (Miller and McCleave, 1994; Munk et al., 2010). Recent evidence also points to elevated copepod abundance and egg production (Andersen et al., 2011), but not primary production (Riemann et al., 2011), within the STCZ.

Copepods are important drivers of carbon and nutrient fluxes in the Sargasso Sea (Deevey, 1971; Roman et al., 1993; Steinberg et al., 2000). Conventional sampling protocols often assume all copepods are alive (e.g. Böttger, 1982; Steinberg et al., 2001). However, there has been increasing recognition that a considerable fraction of *in situ* copepods are in fact carcasses (e.g. Weikert, 1977; Geptner et al., 1990; Böttger-Schnack, 1996; Yamaguchi et al., 2002; Tang et al., 2006a), and ignoring the live/dead status of the specimens could lead to considerable errors in understanding their population dynamics and related ecological processes (Elliott and Tang, 2011). To our knowledge, there has been only one report of copepod carcasses in the bathypelagic layer (2,000–4,000 m) of the Sargasso Sea (Wheeler 1967), whereas the occurrence of copepod carcasses in the upper layer has not been investigated. Upon death, the carcasses can become hotspots for microbial activities (Tang et al., 2009; Bickel and Tang, 2010), be recycled in the upper layers, or transport carbon to the deep waters via sinking (Sampei et al., 2009, 2012; Frangoulis et al., 2011). Hence, knowledge on microbial colonization and rates of carcass degradation is critical for assessing the fate and vertical distribution of carcass-associated carbon and nutrients.

In the present study, we investigated the copepod distributions as well as their live/dead compositions across the North Atlantic STCZ. Recent studies have suggested elevated plankton abundance in this dynamic region (Andersen et al., 2011; Riemann et al., 2011), but the live/dead composition of the zooplankton community remains unknown. Furthermore, we tested how copepod carcass decomposition influences microbial respiration and community succession using shipboard experiments, which allowed us to examine the impacts of carcasses on the microbial community and energy budget in this oligotrophic region (Williams, 1998). Finally, we combined our field and experimental data to examine the influences of copepod carcasses on carbon flux estimates, which we then compared against flux values in the literature to assess the contribution of sinking carcasses to the overall carbon flux.

METHOD

Cruise track and hydrography

This study was conducted in March–April 2014 on board the RV Dana (National Institute of Aquatic Resources, Denmark) in areas of the North Atlantic STCZ as a part of the larger SARGASSO-EEL project (Fig. 1). Transects were positioned to cover the expected area of European eel larvae distribution (Munk et al., 2018). At each station along the transects, hydrographic vertical profiles were obtained by lowering a Seabird® 9/11 CTD from the surface to 400 m depth. Sea surface temperature (SST) information for a larger area of the North Atlantic was obtained from the Operational Sea Surface Temperature and Sea Ice Analysis project (OSTIA,

93 http://ghrsst-pp.metoffice.com). Contours of water column temperatures and SST were generated by
94 an interpolation procedure using inverse distance method in the program Surfer®.
95
96 **Copepod carbon biomass and live/dead composition**
97 Zooplankton were collected using an opening-closing MIDI Multinet® equipped with five nets
98 of 50-µm mesh and a 0.125 m^2 opening. We used a smaller than usual mesh size to avoid under-
99 sampling small life stages and species (Tang et al., 2011) that are common in this region (Andersen
100 et al., 2011). The Multinet was lowered to 400 m, and hauled vertically to the surface at a speed of
101 10 m min^{-1}. Sampling was done at thirty-seven stations in five depth strata: 400–300 m, 300–200 m,
102 200–100 m, 100–50 m and 50–0 m. A total of 250 zooplankton samples were collected. Upon net
103 retrieval, a subsample (ca. 10%) from each cod-end was transferred to a container for live/dead
104 sorting using the Neutral Red staining method. This method, originally developed by Dressel et al.
105 (1972), later improved by Elliott and Tang (2009) and further evaluated by Zetsche and Meysman
106 (2012), allows researchers to quickly and easily distinguish between live and dead copepods. Each
107 subsample was incubated with Neutral Red solution for 20 min in the dark at room temperature.
108 Afterward, the stained subsamples were concentrated on a 50-µm sieve and back-washed with
109 filtered seawater onto a petri dish. Under a stereomicroscope the copepods were counted as live
110 (stained red) or dead (unstained and without vital signs; some showing signs of decomposition).
111 Molts appeared completely transparent and were not counted. Species compositions were not
112 recorded for the live/dead counts due to time constraints. Only copepods were included in live/dead
113 counts because they were the majority of the mesozooplankton in our samples (ca. 75% of
114 estimated total zooplankton carbon biomass), and because the staining method works best on
115 copepods (Elliott and Tang, 2009).
116 After live/dead counting, the subsamples were added to the remainder of the corresponding
117 cod-end content and preserved in 4% buffered formaldehyde. The preserved samples were
118 identified and enumerated by the Arctic Agency (Poland). For each species and life stage, 10
119 individuals (when present) were sized and their body carbon contents were estimated from
120 published algorithms (Table 1). Carcass carbon biomasses were calculated as total copepod carbon
121 biomasses multiplied by the percentages of dead copepods. This is likely to overestimate the carcass
122 biomass as the carbon content of carcasses would be decreased by decomposition, and the carcasses
123 which had sunk farther from their depth of origin would have a lower carbon mass than new
124 carcasses. However, since the depth of origin of the carcasses was not known, it was not possible to
125 include a decomposition factor to the estimates of carcass biomass, particularly since the majority
126 of the zooplankton population at several stations appeared to be evenly distributed throughout the
127 0–200 m depth (see RESULTS), and the decomposition time of carcasses would thus be likely to

differ. Because most of the carcasses collected at depths appeared to be intact, we therefore assumed that the majority of carcasses were collected close to their origin, and had a carbon content equal to live copepods. To constrain the uncertainty associated with this assumption, we used our experimental carcass decomposition rates (see next section) to estimate the expected depth distributions of carcass carbon by assuming a maximum decomposition time in situ (i.e. assuming all carcasses originated at 0 m; see DISCUSSION).

To better illustrate the spatial variations in total copepod carbon biomass (live + dead), we binned the data based on longitudes (ca. every 3° West to East) and latitudes (every 2° North to South).

Copepod carcass decomposition experiments

Carcass decomposition experiments were conducted at three locations (Fig. 1) with the copepod *Oncaea* spp. They were the most numerically abundant in samples sorted for the experiments, making up approximately one-third of the organisms in all samples. Copepods were collected by towing a 45-µm plankton net from just below the fluorescence maximum (FM; based on CTD measurements) to the surface. Individuals of *Oncaea* spp. (size 200–500 µm) were sorted into 5-L bottles containing 0.2-µm filtered seawater, and kept at *in situ* temperature for up to 24 h before the experiments. Another subsample of ca. 100 copepods was measured under an inverted microscope for body lengths (precision ±20 µm). To produce fresh carcasses for the experiments, actively moving copepods were killed by brief exposure (a few seconds) to 10% HCl, then rinsed with filtered seawater and added to the incubation bottles. Water for incubations was obtained from 5–10 m depth, immediately reverse filtered through a 20-µm mesh and added to thirty-two 1-L polypropylene bottles. To twenty of these bottles, 30–40 freshly killed copepods were added; the other twelve bottles without carcasses were used as controls. Incubations were done on a slowly rotating plankton wheel at 22 °C and *in situ* day-night cycles of 30 µmol photons m^{-2} s^{-1} light intensity. At 0, 6, 12 and 24 h, five replicates of carcass bottles and triplicate control bottles were sacrificed for measurements of bacterial community composition and respiration.

Bacterial community composition in carcass decomposition experiments

In the following sections, the different bacterial samples are described as ‘carcass’ (bacteria attached to the carcasses), ‘carcass water’ (free-living bacteria in water where carcasses were incubated), or ‘control water’ (free-living bacteria in the controls).

At each time point of the carcass decomposition experiments, triplicate samples of carcasses (10 each) were gently washed in 0.2 µm-filtered seawater and transferred into Eppendorf tubes.

About 1 L of 'carcass water' (5 replicates) and 'control water' (3 replicates) taken at time 0 and 24 h were filtered onto Supor 0.2 µm filters and stored at -80 °C until processing.

DNA was extracted using the E.Z.N.A.® Tissue DNA Kit (Omega Bio-Tek, Inc.) and quantified using Quant-IT PicoGreen (Invitrogen). Bacterial and Archaeal 16S rRNA genes were PCR amplified using MyTag DNA polymerase (Saveen & Verner AB), 2 µL template, and Illumina primers 515f (GCGTGCCAGCMGCCGCGGTAA) and 806r (GGACTACHV-GGGTWTCTAAT) complemented with sample-specific barcodes (Bates et al., 2010) in 25 µl reaction volumes. In addition, 10 µg μL^{-1} bovine serum albumin (Sigma-Aldrich) and 5 mM $MgCl_2$ (DNA Diagnostic) were added to the 'carcass' samples to facilitate PCR amplification. The PCR cycling condition were: 95°C for 2 min, 29 cycles of: 95°C for 0.30 min, 54°C for 0.30 min, 72 °C for 1.30 min. For each sample, triplicate PCR products were pooled, purified using the Agencourt AMPure XP kit (Beckman coulter Inc.), and quantified. The 84 samples were mixed in equimolar amounts and sequenced (Illumina MiSeq, National High-throughput DNA sequencing Centre, University of Copenhagen, Denmark). Sequence reads were assembled, trimmed to a mean length of 252 nucleotides, and de-multiplexed using the software QIIME v1.9 (Caporaso et al., 2010). Removal of singletons and clustering at 97% similarity was done in USEARCH v1.8 (Edgar, 2010) using the UPARSE-OTU algorithm (Edgar, 2013) with implicit chimera check. Taxonomy was assigned in QIIME using UCLUST (Edgar, 2010) and the Greengenes v.13.8 reference database (McDonald et al., 2012). Chloroplasts and mitochondrial reads were removed before subsequent analysis. The total operational taxonomic units (OTU) were subsampled by randomly picked OTUs to accommodate for the lowest number of sequences found in a sample (4401 sequences $sample^{-1}$) in QIIME.

Phylogenetic similarity between samples was determined by principal component analyses using square root transformed Bray-Curtis dissimilarity distances on OTUs relative abundance < 0.1% in Primer 6.1.7 (Primer-E). To identify the OTUs contributing to dissimilarity between 0 and 24 h old samples, a SIMPER analysis (Clarke and Warwick, 2001) was performed on the above dissimilarity distances.

Respiration during carcass decomposition

Respiration rate was measured as decrease in dissolved oxygen over time in a gas-tight glass chamber (2 mL) using a protected microsensor (Unisense), which registered the oxygen concentration in 2 s intervals. The glass chamber was submerged in a 22°C water bath. Prior to measurements, baseline was established using 0.2-µm filtered seawater. At each time point 4–5 carcasses were transferred from the incubation bottle to the chamber, and measurements were carried out until the dissolved oxygen decreased at <1 mg L^{-1} min^{-1}. Respiration rate (µg O_2 carcass^{-}

197 ^{1} d^{-1}) was calculated from linear regression of the slope (significant at $p < 0.001$) after correction for
198 baseline drift. The daily total respiration was calculated as the sum of time-integrated respirations
199 over the three sampling intervals. Microbial oxygen consumption was then converted to microbial
200 carbon consumption (respiration + production) assuming 1: 1 O_2-to-C molar ratio and 30% bacterial
201 growth efficiency (Del Giorgio and Cole, 1998). The copepod's body volume was estimated from
202 its linear dimensions as 9.87×10^{7} μm^3, which was then converted to a carbon content of 12.8 μg C
203 $copepod^{-1}$ (Hansen et al., 1997). Dividing the daily carbon consumption by the carcass carbon
204 content gave the daily carcass-carbon turnover.
205
206 **RESULTS**
207 **Hydrographical conditions**
208 The water column thermal structure showed distinct changes when crossing the frontal zone,
209 with a sharp incline of the isotherm from the thermocline depth (ca. 200 m) to the surface, most
210 noticeably in the southern sections of the transects (Fig. 2). The influence of colder water masses
211 was more conspicuous to the north of the front. Salinity ranged from about 36.6 at the surface to
212 36.4 at 400 m, with an intrusion of higher salinity water of up to 36.9 in the depth interval of 80–
213 180 m (Munk et al., 2018).
214
215 **Copepod carbon biomass and live/dead compositions**
216 Copepods were the most numerically abundant taxa at all stations. Copepod carbon biomasses
217 were highest within 0–200 m (up to 99 mg C m^{-2}) and slightly higher in the northernmost stations
218 (Fig. 3). The carbon biomass at depths > 200 m was much lower, and was typically less than 15%
219 of that at depths < 200 m.
220 Neutral Red staining revealed that copepod carcasses were present in all samples (Fig. 4).
221 Longitudinally, the proportional abundances of dead copepods (as % dead) appeared to increase
222 toward the east; whereas latitudinally, it was slightly lower in the southern-most stations. The %
223 dead copepods increased with depth, most noticeably below 200 m. Nevertheless, the higher total
224 copepod carbon biomasses at 0–200 m resulted in considerably larger amounts of carcass carbon
225 biomass in the upper layer across the latitudes and longitudes (Fig. 5).
226
227 **Carcass decomposition experiments - Bacterial composition and respiration**
228 The bacterial communities were dominated by Gammaproteobacteria, Alphaproteobacteria and
229 Bacteroidetes (Supplementary materials Fig. S1). Bacterial community compositions in "control
230 water" and "carcass water" were similar, whereas "carcass" samples clearly differed from the other
231 two, apart from a small overlap (Supplementary material Fig. S2). A pronounced succession led to

an increasingly distinct carcass-associated bacterial community composition over time (Supplementary materials Fig. S1).

SIMPER analysis showed that Rickettsiales and Pseudomonadales accounted for most of the dissimilarity between 0 and 24 h in Exp. 1, but in opposite manner: Rickettsiales increased in relative abundance over time, whereas Pseudomonadales decreased (Supplementary material Table S1). On the contrary, Rickettsiales decreased over time in Exp. 2 and 3, whereas Pseudomonadales increased in Exp. 2. In both Exp. 2 and 3, Vibrionales proliferated and contributed substantially to the dissimilarity (Supplementary material Table S1).

Microbial respiration rates associated with carcass decomposition increased with time (Table 2). The integrated daily respiration rate was considerably lower in Exp. 2 than in the other two experiments. The estimated carcass-carbon turnover varied from 18 to 93% per day, with an average of 56.5% d^{-1} (Table 2).

DISCUSSION

Zooplankton sampling at the Sargasso Sea BATS station has been on-going for nearly three decades, generating detailed temporal information of the larger zooplankton (200-μm net) communities as influenced by the oceanographic conditions (Steinberg et al., 2001). However, like many sampling programs, whether the zooplankton are live or dead upon collection has not been taken into account. Here, we show that copepod carcasses were prevalent in the STCZ. Within the upper 200 m, where zooplankton tend to exert the strongest grazing impacts (Roman et al., 1993; Steinberg et al., 2001), 14–19 % of the copepod biomass was carcasses when assuming the same carbon content for carcasses as for live copepods. Even if we assume an average decomposition time of 24 h, hence ca. 57% of carbon loss to decomposition, carcasses would still account for 6–8% of the biomass within the upper 200 m. In both cases, carcasses comprised a considerable fraction of the total copepod biomass. Occurrence of carcasses implicates non-predation mortality factors at work (Tang et al., 2014), although pin-pointing the actual cause(s) is beyond the scope of this study. Nevertheless, the presence of carcasses can have important ramifications for the regional biogeochemistry, as discussed below.

Similar to other detritus (e.g. marine snow, fecal pellets), copepod carcasses provide organic-rich loci for bacteria in the otherwise oligotrophic Sargasso Sea (Carlson and Ducklow, 1996). In our experiments, ambient bacteria rapidly colonized and exploited copepod carcasses leading to an increase in microbial respiration. Concurrently, there was a shift in the carcass-associated bacterial community composition, consistent with previous observations that carcass decomposition favors certain bacterial groups (Tang et al., 2006b). In particular, members of Rickettsiales, Pseudomonadales and Vibrionales—well adapted to high carbon concentrations—proliferated

substantially during carcass decomposition. It is noteworthy that the predominance of specific OTUs (e.g. the lack of responsive Vibrionales in Experiment 1; Supplementary material Table S1) and the estimated respiration rate (Table 2) varied considerably between experiments. Although the incubations were done under the same temperature and light conditions, the copepods and the incubation waters were taken from different locations for the different experiments, and they carried different initial microbial communities (Supplementary material Fig. S1), which likely resulted in different microbial successions and activity levels (Moisander et al., 2015). Similar to bacterial communities on live copepods (e.g. Dziallas et al., 2013; De Corte et al., 2014; Shoemaker and Moisander, 2015), communities associated with carcasses were distinct relative to those in the seawater, although with an overlap for a few samples (Fig. S2). Interestingly, we noted the appearance of several low-abundance anaerobic taxa towards the end of the incubations (data not shown). Hence, it appears that carcasses were colonized by a subset of the free-living bacterial community, which developed into a rather distinct assemblage over time as the carcass-associated environmental conditions changed, including the potential development of micro-anoxic zones (Glud et al., 2015).

Our calculations of microbial oxygen consumption and carcass-carbon turnover in the decomposition experiments relied on a number of assumptions: We assumed that all carcass carbon was equally labile, but the different organic fractions would likely degrade at different rates (Tang et al., 2009; Bickel and Tang, 2010). We also assumed that decomposition was entirely aerobic, but in reality anaerobic decomposition could occur (Glud et al., 2015). Nevertheless, the calculated carcass-carbon turnover rates in Exp. 1 and 2 were comparable to those reported by others (Lee and Fisher, 1992; Tang et al., 2009). The rate was considerably higher in Exp. 3, but similarly high turnover rates have been observed for the protein fraction of copepod carcasses (Bickel and Tang, 2010), and carbon loss could also be accelerated by carcass fragmentation and leakage (Tang et al., 2009).

Contributions of copepod carcasses to epipelagic respiration vs. sinking fluxes would depend on their depths of origin and residence times above the thermocline. From the literature, gravitational sinking velocity of copepod carcasses of comparable size in 25 °C seawater with a salinity of 35 is ca. 90 m d^{-1} (Elliott et al., 2010). If we conservatively assume that all copepod deaths occurred at 0 m and the carcasses began their descent, based on our measured microbial respiration rates, the carcasses could lose on average 57–100 % of their carbon to microbial decomposition within 0–200 m, with the rest (0–43%; average 22%) potentially exported to below the thermocline. Clearly, not all if any carcasses originated from 0 m, and 0% carcass export cannot be correct because carcasses were present in 200–400 m. The fact that most of the carcasses collected below the thermocline were intact suggests that many of them originated at depths and

that our calculation may have over-estimated carcass decomposition. Nevertheless, despite the uncertainty in our calculations, the estimated average carcass carbon export (22%) is consistent with our field data at least at the population level (Fig. 5): The estimated carcass carbon biomass in the 200–400 m layer was equal to 23–29% of that in the 0–200 m layer.

Carcass decomposition will add to the system's oxygen consumption, but it is ignored in conventional bulk-water respiration measurements. We calculated the carcass-driven respiration as *in situ* carcass carbon biomasses multiplied by the average carcass carbon-specific respiration rate determined in the experiments (Table 3). The estimated carcass-driven respiration is at least 2–3 orders of magnitude lower than the ambient respiration rates reported in the literature (Table 3). Therefore, copepod carcasses are a negligible oxygen sink, and their presence would not significantly impact the overall autotrophy-heterotrophy balance in the Sargasso Sea.

In addition to being important trophic links within the pelagic food web, zooplankton can also influence vertical transportation of material via vertical migration (active flux) and via sinking carcasses and fecal pellets (passive flux). The contribution by migrating zooplankton to the active carbon flux in the Sargasso Sea is of particular interest, as it has been proposed as an explanation for the spring-fall carbon imbalance (Steinberg et al., 2000). In field studies, active flux is often derived from the night/day differential in zooplankton biomass within the mixed layer, which represents the zooplankton biomass that migrates downward, and which via respiration and excretion releases carbon at depth (e.g. Dam et al., 1995; Steinberg et al., 2000). From this, Dam et al. (1995) calculated a migratory carbon flux equivalent to an average of 34% of the gravitational particulate carbon (POC) flux in the upper 150 m at BATS, whereas Steinberg et al. (2000) estimated that migratory carbon flux accounts for 7.8–14.4 % (mean) of the POC flux within the upper 300 m. The underlying assumption that all zooplankton in the mixed layer are alive (a pre-requisite for "active" flux) was not verified in those studies, but violation to this assumption would mean an overestimation of the active flux. Within the upper 300 m, we observed an average of 15% (across latitudes) to 22% (across longitudes) dead copepods, and these percentages need to be taken into account when calculating the active flux. It should be noted that the zooplankton community compositions at BATS are different from our observations in the STCZ partly due to the use of different mesh sizes (200 μm vs. 50 μm), and we did not identify migratory vs. non-migratory species in our live/dead sorting. Nevertheless, the percentages of dead copepods (15–22%) are of similar magnitude as the migratory flux percentage estimate by Dam et al. (1995) and Steinberg et al. (2000). Therefore, the migratory flux could have been overestimated in the previous studies when the zooplankton live/dead status in the mixed layer was not considered.

Instead of the active flux, carcasses can be a part of the passive detrital flux. In our study, carcasses were concentrated in the upper 200 m, but some intact carcasses were still present below

337 the thermocline (Fig. 5), which could readily contribute to the passive POC flux to depth. Although
338 there are no available POC flux data for the STCZ, we may use data from BATS to speculate on the
339 importance of carcass carbon flux. We estimated an average carcass carbon biomass of 0.82–1.44
340 mg C m^{-2} in the 200–300 m layer, and 0.87–1.05 mg C m^{-2} in the 300–400 m layer in the STCZ
341 (Fig. 5). According to an earlier study, POC flux at BATS was 13.9 mg C m^{-2} d^{-1} at 300 m, and 8.7
342 mg C m^{-2} d^{-1} at 600 m (Steinberg et al., 2000). Carcass sinking rate is unknown and is highly
343 influenced by decomposition state and turbulence (Kirillin et al., 2012). Assuming a carcass sinking
344 rate of 90 m d^{-1} for our hydrographical conditions (Elliott et al., 2010), the carcasses could
345 contribute ca. 6–10 % of the POC flux at 300 m, and 5–6 % at 600 m. These, coincidentally, are
346 comparable to the estimated migratory active flux at similar depths at BATS (Steinberg et al.,
347 2000).
348 Other researchers, using different methods, have also shown significant contributions of
349 zooplankton carcasses to passive carbon flux elsewhere. For example, copepod carcasses
350 contributed on average 36% of the annual total passive carbon flux in the Beaufort Sea (Sampei et
351 al., 2009), and up to 91% in the Amundsen Gulf during the post-bloom period (Sampei et al., 2012).
352 Copepod carcass carbon flux exceeded even the fecal pellet carbon flux on most occasions in the
353 Bay of Calvi (Frangoulis et al., 2011). While our simple calculations ignore the effects of
354 decomposition and necrophagy in the mesopelagic layer (Elliott et al. 2010), our study as well as
355 others show that knowledge of the zooplankton live/dead composition may reveal an unexpected
356 carbon flow pathway via passively sinking zooplankton carcasses, instead of or in addition to active
357 transport by vertical migrators.
358
359 **CONCLUSIONS**
360 The dynamic nature of the STCZ was illustrated by the distinct latitudinal variations in the
361 water column thermal structure across the front. Within the STCZ, copepod carcasses were
362 ubiquitous and their biomass was concentrated in the upper 200 m. Our experiments showed that
363 copepod carcasses were colonized by specialized bacterial taxa and rapidly degraded by microbial
364 activity. While decomposing carcasses overall constitute a negligible oxygen sink in the STCZ,
365 sinking copepod carcasses provide an alternative carbon transport pathway comparable in
366 magnitude to conventional zooplankton migratory flux. Inclusion of data on *in situ* live/dead
367 compositions of copepods and other zooplankton may therefore lead to a different understanding of
368 active (migratory zooplankton) vs. passive (sinking carcasses) carbon flux to the deep waters, as
369 well as other zooplankton-driven biogeochemical processes in the STCZ.
370

ACKNOWLEDGEMENTS

The authors thank the crew of the RV Dana for assistance. This study was supported by funds from the Carlsberg Foundation, Denmark (CF 2012_01_0272) and the Danish Centre for Marine Research (DCH 2013-02) awarded to PM. HPG was supported by funds from the Leibniz Society and DFG (GR1540/23-1 & 29-1). Reviewers and editor provided constructive comments to improve the manuscript.

Authors' contributions: All authors contributed to conceiving the idea, collecting the data, and analyzing the data. KWT wrote the manuscript with input from co-authors.

381 **REFERENCES**

382 Andersen, N.G., Nielsen, T.G., Jakobsen, H.H., Munk, P. and Riemann, L. (2011) Distribution and
383 production of plankton communities in the subtropical convergence zone of the Sargasso Sea.
384 II. Protozooplankton and copepods. *Mar. Ecol. Prog. Ser.*, **426,** 71–86.
385 Aristegui, J., Agusti, S., Middelburg, J.J. and Duarte, C.M. (2005a) Respiration in the mesopelagic
386 and bathypelagic zones of the oceans. In: Del Giorgio, P.A. and Williams, P.J.L.B. (ed.)
387 *Respiration in aquatic ecosystems.* Oxford University Press, USA, pp. 181–205.
388 Aristegui, J., Duarte, C.M., Gasol, J.M. and Alonso-Sáez, L. (2005b) Active mesopelagic
389 prokaryotes support high respiration in the subtropical northeast Atlantic Ocean. *Geophy. Res.*
390 *Lett.,* **32,** L03608.
391 Bates, S. T., Berg-Lyons, D., Caporaso, J. G., Walters, W. A., Knight, R. and Fierer, N. (2010)
392 Examining the global distribution of dominant archaeal populations in soil. *ISME Journal,* **5,**
393 908–917.
394 Berggreen, U., Hansen, B. and Kiørboe, T. (1988) Food size spectra, ingestion and growth of the
395 copepod *Acartia tonsa* during development: implications for determination of copepod
396 production. *Mar. Biol.,* **99,** 341–352.
397 Bickel, S.L. and Tang, K.W. (2010) Microbial decomposition of proteins and lipids in copepod
398 versus rotifer carcasses. *Mar. Biol.,* **157,** 1613–1624.
399 Böttger, R. (1982) Studies on the small invertebrate plankton of the Sargasso Sea. *Helgoländer*
400 *Meeresunters,* **35,** 369–383.
401 Böttger-Schnack, R. (1996) Vertical structure of small metazoan plankton, especially noncalanoid
402 copepods. I. Deep Arabian Sea. *J. Plankton Res.,* **18,** 1073–1101.
403 Caporaso, J.G., Kuczynski, J., Stombaugh, J., Bittinger, K., Bushman, F.D., Costello, E.K., Fierer,
404 N., Pena, A.G., et al. (2010) QIIME allows analysis of high-throughput community
405 sequencing data. *Nature Methods*, **7,** 335–336.
406 Carlson, C.A. and Ducklow, H.W. (1996) Growth of bacterioplankton and consumption of
407 dissolved organic carbon in the Sargasso Sea. *Aquat. Microb. Ecol.,* **10,** 69–85.
408 Carr, M.E., Friedrichs, M.A., Schmeltz, M., Aita, M.N., Antoine, D., Arrigo, K.R., Asanuma, I.,
409 Aumont, O., et al. (2006) A comparison of global estimates of marine primary production
410 from ocean color. *Deep-Sea Res. II,* **53,** 741–770.
411 Chisholm, L.A. and Roff, J.C. (1990) Size-weight relationships and biomass of tropical neritic
412 copepods off Kingston, Jamaica. *Mar. Biol.,* **106,** 71–77.
413 Clarke, K.R. and Warwick, R.M. (2001) *Change in marine communities: an approach to statistical*
414 *analysis and interpretation.* PRIMER-E, Plymouth.

415 Dam, H.G., Roman, M.R. and Youngbluth, M.J. (1995) Downward export of respiratory carbon and
416 dissolved inorganic nitrogen by diel-migrant mesozooplankton at the JGOFS Bermuda time-
417 series station. *Deep-Sea Res. I,* **42,** 1187–1197.
418 Deevey, G.B. (1971) The annual cycle in quantity and composition of the zooplankton of the
419 Sargasso Sea off Bermuda I. The upper 500 m. *Limnol. Oceanogr.,* **16,** 219–240.
420 De Corte, D., Lekunberri, I., Sintes, E., Garcia, J.A.L., Gonzales, S. and Herndl, G.J. (2014)
421 Linkage between copepods and bacteria in the North Atlantic Ocean. *Aquat. Microb. Ecol.,*
422 **72,** 215–225.
423 Del Giorgio, P.A. and Cole, J.J. (1998) Bacterial growth efficiency in natural aquatic systems. *Ann.*
424 *Rev. Ecol. Syst.,* **29,** 503–541.
425 Dressel, D.M., Heinle, D.R. and Grote, M.C. (1972) Vital staining to sort dead and live copepods.
426 *Chesapeake Sci.,* **13,** 156–159.
427 Ducklow, H.W. and Doney, S.C. (2013) What is the metabolic state of the oligotrophic ocean? A
428 debate. *Annu. Rev. Mar. Sci.,* **5,** 525–533.
429 Dziallas, C., Grossart, H.-P., Tang, K.W. and Nielsen, T.G. (2013) Distinct communities of free-
430 living and copepod-associated microorganisms along a salinity gradient in Godthåbsfjord,
431 West Greenland. *Arctic Antarc. Alpine Res.,* **45,** 471–480.
432 Edgar, R. C. (2010) Search and clustering orders of magnitude faster than BLAST. *Bioinformatics,*
433 **26,** 2460–2461.
434 Edgar, R. C. (2013) UPARSE: highly accurate OTU sequences from microbial amplicon reads.
435 *Nature Methods,* **10,** 996–998.
436 Elliott, D.T. and Tang, K.W. (2009) Simple staining method for differentiating live and dead marine
437 zooplankton in field samples. *Limnol. Oceanogr. Methods,* **7,** 585–594.
438 Elliott, D.T. and Tang, K.W. (2011) Influence of carcass abundance on estimates of mortality and
439 assessment of population dynamics in *Acartia tonsa*. *Mar. Ecol. Prog. Ser.,* **427,** 1–12.
440 Elliott, D.T., Harris, C.K. and Tang, K.W. (2010) Dead in the water: The fate of copepod carcasses
441 in the York River estuary, Virginia. *Limnol. Oceanogr.,* **55,** 1821–1834.
442 Frangoulis, C., Skliris, N., Lepoint, G., Elkalay, K., Goffart, A., Pinnegar, J.K. and Hecq, J.H.
443 (2011) Importance of copepod carcasses versus feacal pellets in the upper water column of an
444 oligotrophic area. *Estuar. Coast. Shelf Sci.,* **92,** 456–463.
445 Geptner, M.V., Zaikin, A.N. and Rudyakov, Y.A. (1990) Dead copepods in plankton: Facts and
446 hypotheses. *Oceanology,* **30,** 99–102.
447 Glud, R.N., Grossart, H.-P., Larsen, M., Tang, K.W., Arendt, K.E., Rysgaard, S., Thamdrup, B. and
448 Nielsen, T.G. (2015) Copepod carcasses as microbial hotspots for pelagic denitrification.
449 *Limnol. Oceanogr.,* **60,** 2026–2036.

450 Hansell, D.A., Bates, N.R. and Gundersen, K. (1995) Mineralization of dissolved organic carbon in
451 the Sargasso Sea. *Mar. Chem.,* **51,** 201–212.
452 Hansen, P.J., Bjørnsen, P.K. and Hanse, B.W. (1997) Zooplankton grazing and growth: Scaling
453 with the 2-2,000 μm body size range. *Limnol. Oceanogr.,* **42,** 687–704.
454 Hopcroft, R.R., Roff, J.C. and Lombard, D. (1998) Production of tropical copepods in Kingston
455 Harbour, Jamaica: the importance of small species. *Mar. Biol.,* **130,** 593–604.
456 Karl, D.M. and Lukas, R. (1996) The Hawaii Ocean Time-series (HOT) program: Background,
457 rationale and field implementation. *Deep-Sea Res. II,* **43,** 129–156.
458 Kirillin, G., Grossart, H.-P. and Tang, K.W. (2012) Modeling sinking rate of zooplankton carcasses:
459 Effects of stratification and mixing. *Limnol. Oceanogr.,* **57,** 881–894.
460 Lee, B.G. and Fisher, N.S. (1992) Decomposition and release of elements from zooplankton debris.
461 *Mar. Ecol. Prog. Ser.,* **88,** 117–128.
462 McDonald, D., Price, M.N., Goodrich, J., Nawrocki, E.P., DeSantis, T.Z., Probst, A., Andersen,
463 G.L., Knight, R. and Hugenholtz, P. (2012) An improved Greengenes taxonomy with explicit
464 ranks for ecological and evolutionary analyses of bacteria and archaea. *The ISME Journal*, **6,**
465 610–618.
466 Michaels, A.F. and Knap, A.H. (1996) Overview of the U.S. JGOFS Bermuda Atlantic Time-series
467 Study and the Hydrostation S program. *Deep-Sea Res. II,* **43,** 157–198.
468 Miller, M.J. and McCleave, J.D. (1994) Species assemblages of leptocephali in the Subtropical
469 Convergence Zone of the Sargasso Sea. *J. Mar. Res.,* **52,** 743–772.
470 Moisander, P.H., Sexton, A.D. and Daley, M.C. (2015) Stable Associations Masked by Temporal
471 Variability in the Marine Copepod Microbiome. *PLoS ONE,* **10,** e0138967.
472 Mouriño-Carballido, B. and McGillicuddy, D.J., Jr. (2006) Mesoscale variability in the metabolic
473 balance of the Sargasso Sea. *Limnol. Oceanogr.,* **51,** 2675–2689.
474 Munk, P., Hansen, M.M., Maes, G.E., Nielsen, T.G., Castonguay, M., Riemann, L., Sparholt, H.,
475 Als, T.D., et al. (2010) Oceanic fronts in the Sargasso Sea control the early life and drift of
476 Atlantic eels. *Proc. R. Soc. B,* **277,** 3593–3599.
477 Munk, P., Nielsen, T.G., Jaspers, C., Ayala, D. J., Tang, K.W., Lombard, F. and Riemann, L.
478 (2018). Vertical structure of plankton communities in areas of European eel larvae
479 distribution in the Sargasso Sea. *J. Plankton Res.,* **40,** 362–375.
480 Obernosterer, I., Kawasaki, N. and Benner, R. (2003) P-limitation of respiration in the Sargasso Sea
481 and uncoupling of bacteria from P-regeneration in size-fractionation experiments. *Aquat.*
482 *Microb. Ecol.,* **32,** 229–237.
483 Polovina, J.J., Howell, E.A. and Abecassis, M. (2008) Ocean's least productive waters are
484 expanding. *Geophy. Res. Lett.,* **35,** L03618.

485 Roman, M.R., Dam, H.G., Gauzens, A.L. and Napp, J.M. (1993) Zooplankton biomass and grazing
486 at the JGOFS Sargasso Sea time series station. *Deep-Sea Res. I,* **40,** 883–901.
487 Riemann, L., Nielsen, T.G., Kragh, T., Richardson, K., Praner, H., Jakobsen, H.H. and Munk, P.
488 (2011) Distribution and production of plankton communities in the subtropical convergence
489 zone of the Sargasso Sea. I. Phytoplankton and bacterioplankton. *Mar. Ecol. Prog. Ser.,* **426,**
490 57–70.
491 Sampei, M., Sasaki, H., Hattori, H., Forest, A. and Fortier, L. (2009) Significant contribution of
492 passively sinking copepods to downward export flux in Arctic waters. *Limnol. Oceanogr.,* **54,**
493 1894–1900.
494 Sampei, M., Sasaki, H., Forest, A. and Fortier, L. (2012) A substantial export flux of particulate
495 organic carbon linked to sinking dead copepods during winter 2007−2008 in the Amundsen
496 Gulf (southeastern Beaufort Sea, Arctic Ocean). *Limnol. Oceanogr.,* **57,** 90–96.
497 Satapoomin, S. (1999) Carbon content of some tropical Andaman Sea copepods. *J. Plankton Res.,*
498 **21,** 2117–2123.
499 Shoemaker, K.M. and Moisander, P.H. (2015) Microbial diversity associated with copepods in the
500 North Atlantic subtropical gyre. *FEMS Microbiol. Ecol.,* **91,** fiv064.
501 Steinberg, D.K., Carlson, C.A., Bates, N.R., Goldthwait, S.A., Madin, L.P. and Michaels, A.F.
502 (2000) Zooplankton vertical migration and the active transport of dissolved organic and
503 inorganic carbon in the Sargasso Sea. *Deep-Sea Res. I,* **47,** 137–158.
504 Steinberg, D.K., Carlson, C.A., Bates, N.R., Johnson, R.J., Michaels, A.F. and Knap, A.H. (2001)
505 Overview of the US JGOFS Bermuda Atlantic Time-Series Study (BATS): a decade-scale
506 look at ocean biology and biogeochemistry. *Deep-Sea Res. II,* **48,** 1405–1447.
507 Tang, K.W., Freund, C.S. and Schweitzer, C.L. (2006a) Occurrence of copepod carcasses in the
508 lower Chesapeake Bay and their decomposition by ambient microbes. *Estuar. Coast. Shelf*
509 *Sci.,* **68,** 499–508.
510 Tang, K.W., Hutalle, K.M.L. and Grossart, H.P. (2006b) Microbial abundance, composition and
511 enzymatic activity during decomposition of copepod carcasses. *Aquat. Microb. Ecol.,* **45,**
512 219–227.
513 Tang, K.W., Bickel, S.L., Dziallas, C. and Grossart, H.P. (2009) Microbial activities accompanying
514 decomposition of cladoceran and copepod carcasses under different environmental conditions.
515 *Aquat. Microb. Ecol.,* **57,** 89–100.
516 Tang, K.W., Gladyshev, M.I., Dubovskaya, O.P., Kirillin, G. and Grossart, H.-P. (2014)
517 Zooplankton carcasses and non-predatory mortality in freshwater and inland sea
518 environments. *J. Plankton Res.,* **36,** 597–612.

519 Tang, K.W., Nielsen, T.G., Munk, P., Mortensen, J., Møller, E.F., Arendt, K.E., Tönnesson, K.,
520 Pedersen, T.J. (2011) Metazooplankton community structure, feeding rate estimates, and
521 hydrography in a meltwater influenced Greenlandic fjord. *Marine Ecology Progress Series*
522 **434,** 77–90.
523 Weikert, H. (1977) Copepod carcasses in the upwelling region south of Cap Blanc, N.W. Africa.
524 *Mar. Biol.,* **42,** 351–355.
525 Wheeler, E.H. (1967) Copepod detritus in the deep sea. *Limnol. Oceanogr.,* **12,** 697–702.
526 Williams, P.L.B. (1998) The balance of plankton respiration and photosynthesis in the open
527 oceans. *Nature*, **394**, 55.
528 Zetsche, E. M. and Meysman, F. J. (2012) Dead or alive? Viability assessment of micro-and
529 mesoplankton. *J. Plankton Res.,* **34,** 493–509.
530

531 **TABLE LEGENDS**

532

533 Table 1. Algorithms used for size-carbon conversation in this study. L is prosome length; TL is total
534 length; Dry weight (DW) is converted to carbon assuming a C:DW ratio of 0.45.

535

536 Table 2. Microbial respiration during carcass decomposition measured in three time intervals and
537 integrated over 24 hours, as well as the microbial carbon consumption of carcasses and carcass
538 turnover.

539

540 Table 3. Biological oxygen demand reported for Sargasso Sea and the nearby regions. Where
541 necessary, published carbon respiration rates are converted to oxygen consumption rates assuming
542 1:1 C-to-O_2 molar ratio.

543

544 **FIGURE LEGENDS**

545

546 Fig. 1. Chart of SST contoured from satellite observations on 1st April 2014. Isotherms are
547 illustrated in 0.5°C intervals. Transects of sampling stations (dots) are numbered 1–9. Larger circles
548 indicate locations of carcass decomposition experiments.

549

550 Fig. 2. Vertical temperature profiles for transects 1-9 (see Fig. 1) with isotherm interval at 0.5°C.

551

552 Fig. 3. Total copepod carbon biomass (mean + s.d.) in different strata across latitudes (A-E; 31.50°
553 to 24.67°; binned every 2°) and longitudes (F-J; -68.50° to -37.67°; binned very 3°) along the cruise
554 track (see Fig. 1). Note the different y-axis scale for panels D, E, I and J.

555

556 Fig. 4. Proportional abundances of dead copepods (mean + s.d.) in different strata across latitudes
557 (A-E) and longitudes (F-J) along the cruise tracks. Data are binned in the same manner as in Fig. 3.

558

559 Fig. 5. Copepod carcass carbon biomass (mg C m^{-2}; mean + s.d.) for the different strata averaged
560 across latitudes 31.50° to 24.67° (A) and longitudes -68.50° to -37.67° (B), assuming the same
561 carcass carbon content as for live copepods.

562

563

Table 1. Algorithms used for size-carbon conversation in this study. L is prosome length; TL is total length; Dry weight (DW) is converted to carbon assuming a C:DW ratio of 0.45.

Taxa	Stage	Equation	Reference
Copepoda	Nauplii	$mg\ C = 3.18 \times 10^{-12} \times L_{\mu m}^{3.31}$	Berggreen et al. (1988)
Paracalanus, *Clausocalanus* and *Calocalanus*	Copepodites	$\ln(\mu g\ DW) = 3.25 \times \ln(L_{\mu m}) - 19.65$	Chisholm and Roff (1990)
Oithona	Copepodites	$\log(\mu g\ DW) = 3.16 \times \log(L_{mm}) - 8.18$	Hopcroft et al. (1998)
All other Calanoida	Copepodites	$\ln(\mu g\ DW) = 2.74 \times \ln(L_{\mu m}) - 16.41$	Chisholm and Roff (1990)
All other Cyclopoida (incl. *Oncaea*)	Copepodites	$\ln(\mu g\ DW) = 1.96 \times \ln(L_{\mu m}) - 11.64$	Chisholm and Roff (1990)
Harpacticoida	Copepodites	$\ln(\mu g\ C) = 1.15 \times \ln(TL_{\mu m}) - 7.79$	Satapoomin (1999)

Table 2. Microbial respiration during carcass decomposition measured in three time intervals and integrated over 24 hours, as well as the microbial carbon consumption of carcasses and carcass turnover.

	Respiration (μg O_2 $carcass^{-1}$)			Integrated respiration (μg O_2 $carcass^{-1}$ d^{-1})	Carcass-C consumption (μg C $carcass^{-1}$ d^{-1})	O_2 consumption (μgO_2 μg^{-1} C d^{-1})	Carcass-C turnover (% d^{-1})
	0-0.25 d	0.25-0.5 d	0.5-1 d				
Exp 1	1.66	2.13	5.13	8.92	7.43	0.70	57.9
Exp 2	0.27	0.58	1.97	2.82	2.35	0.22	18.3
Exp 3	2.66	4.05	7.63	14.34	11.95	1.12	93.2
			Mean	**8.70**	**7.25**	**0.68**	**56.5**
			S.D.	**5.76**	**4.80**	**0.45**	**37.4**

Table 3. Biological oxygen demand reported for Sargasso Sea and the nearby regions. Where necessary, published carbon respiration rates are converted to oxygen consumption rates assuming 1:1 C-to-O_2 molar ratio.

Depth (m)	Respiration (μmol O_2 m^{-2} d^{-1})	Note	Reference
20	8.8-9.0 $\times 10^3$	24-h incubation	Hansell et al. (1995)
0-75	9.8×10^4 in surface mixed layer; 8.2×10^4	BOD bottle incubation	Obernosterer et al. (2003)
200-1000	4.1×10^3	ETS method	Aristegui et al. (2005a)
Epipelagic	6.4-9.7 $\times 10^4$	Cited N. Navarro pers. comm.	Aristegui et al. (2005b)
Epipelagic	8.9-13.6 $\times 10^4$	Cited Duarte et al. (2001)	Aristegui et al. (2005b)
Mesopelagic (600 and 1000)	350 at 600 m; 80 at 1000 m	Dark bottle incubation + Winkler titration	Aristegui et al. (2005b)
0-100	2-11 $\times 10^4$	Mesoscale eddies; Winkler titration	Mourino-Carballido & McGillicuddy (2006)
0-400	17.5-73.1 (North-South) 18.5-116.5 (West-East)	Estimated carcass-driven respiration	This study

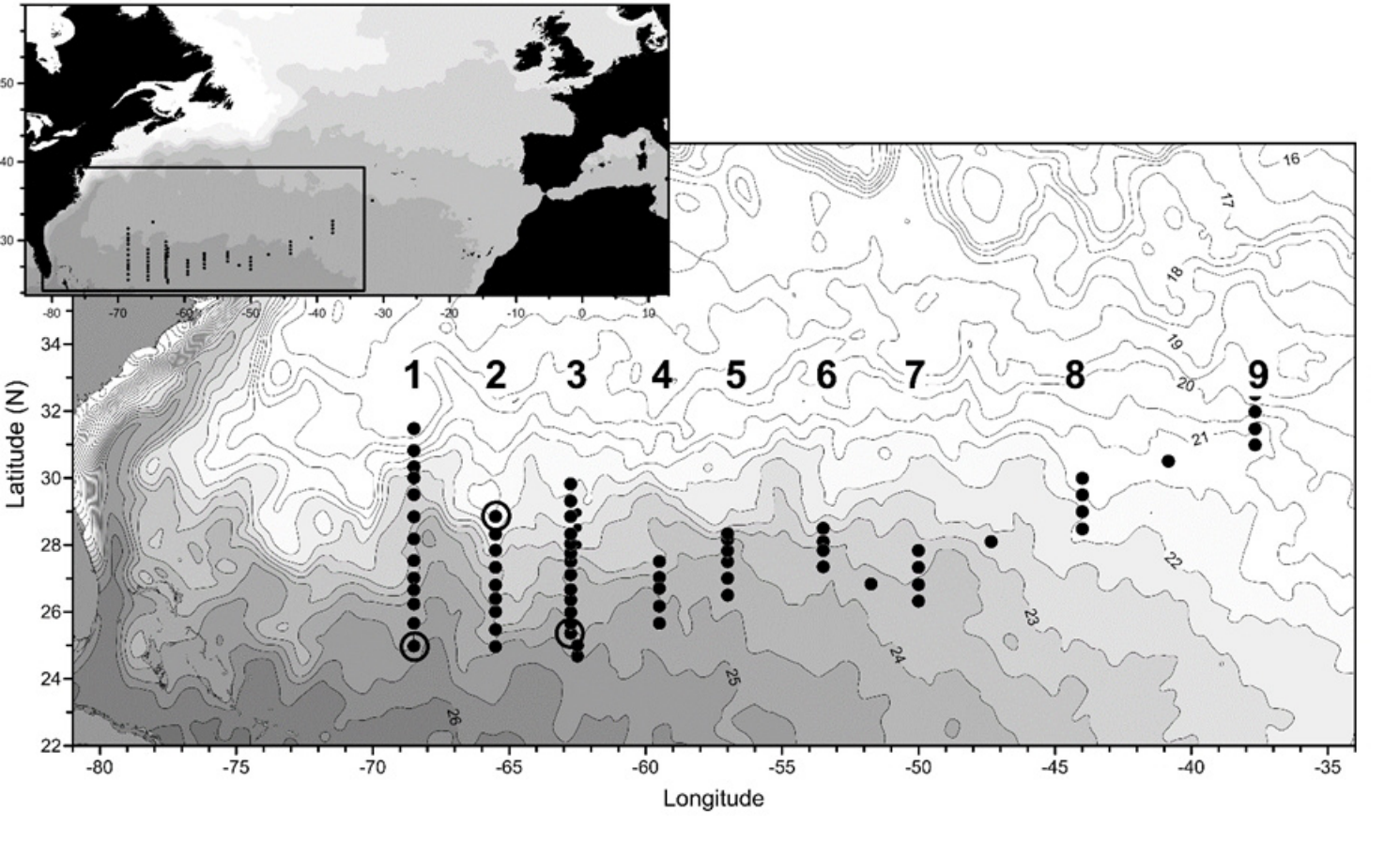
1
2
3
4
5
6
7
8
9
16
17
18
19
20
21
22
23
24
25
26
Latitude (N)
Longitude
-80
-75
-70
-65
-60
-55
-50
-45
-40
-35
22
24
26
28
30
32
34

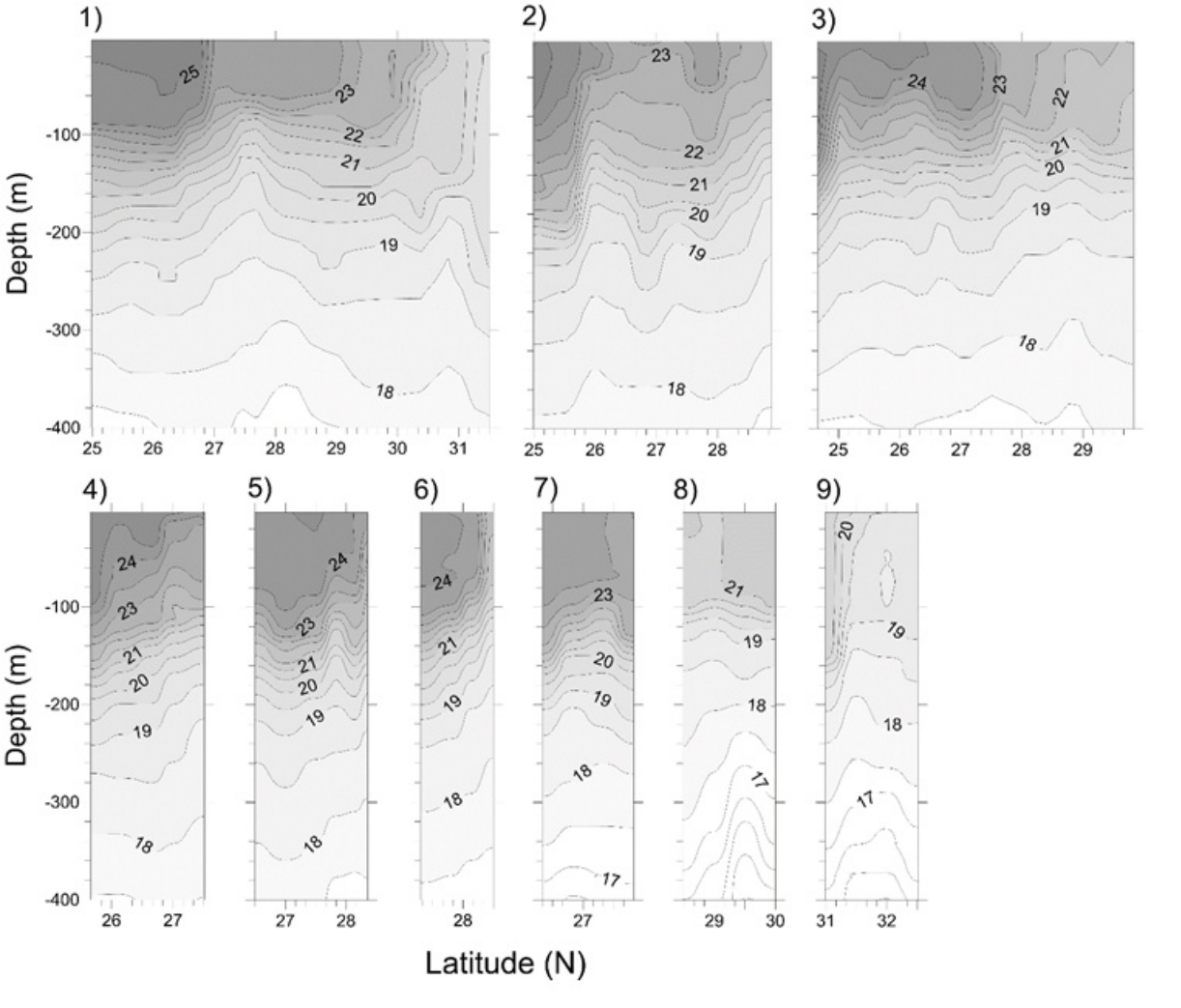
1)
2)
3)
4)
5)
6)
7)
8)
9)
Depth (m)
-100
-200
-300
-400
25
26
27
28
29
30
31
32
Latitude (N)

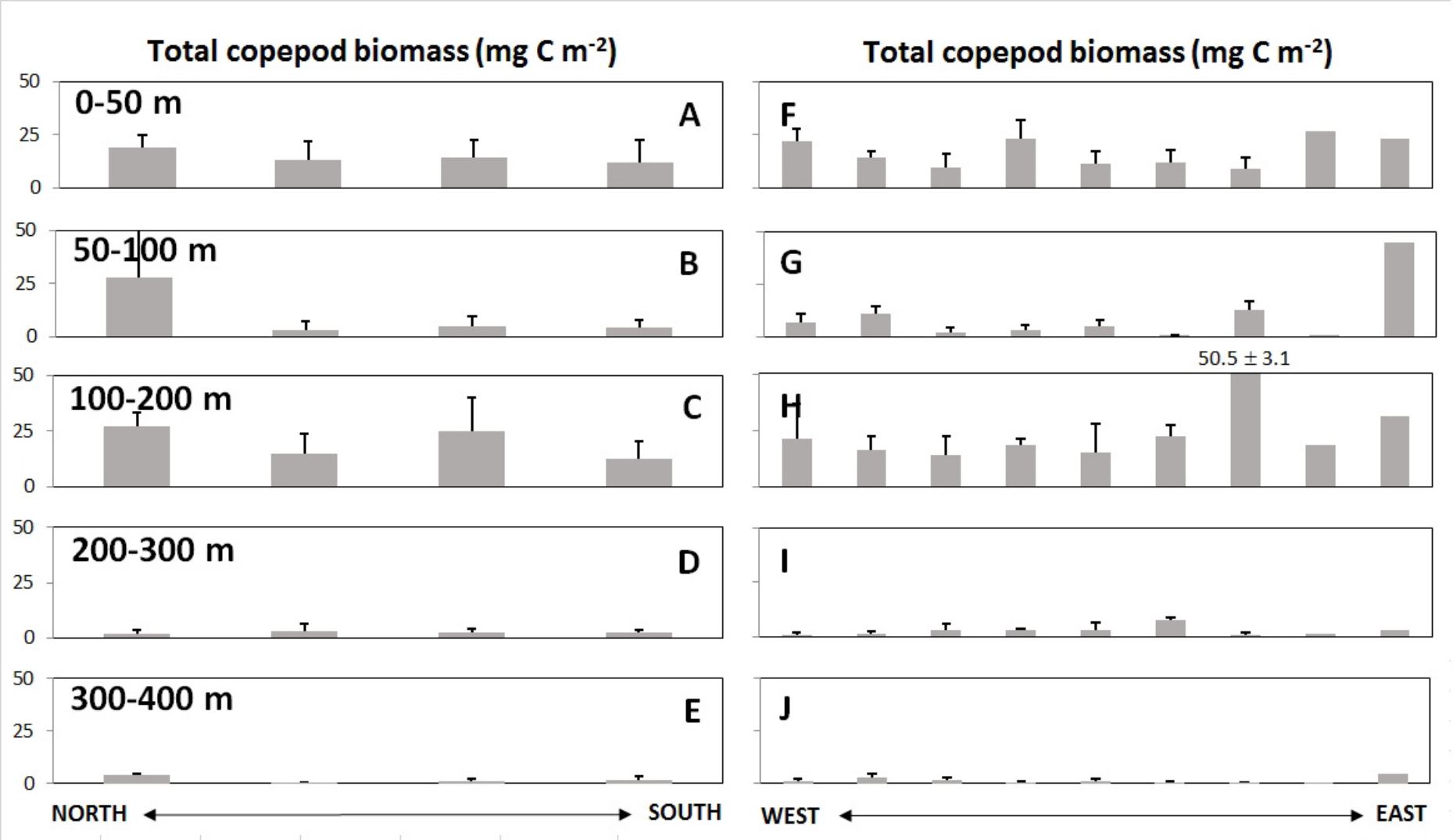
Total copepod biomass (mg C m-2)
Total copepod biomass (mg C m-2)
0-50 m
A
50-100 m
B
100-200 m
C
200-300 m
D
300-400 m
E
F
G
50.5 ± 3.1
H
I
J
50
25
0
NORTH
SOUTH
WEST
EAST

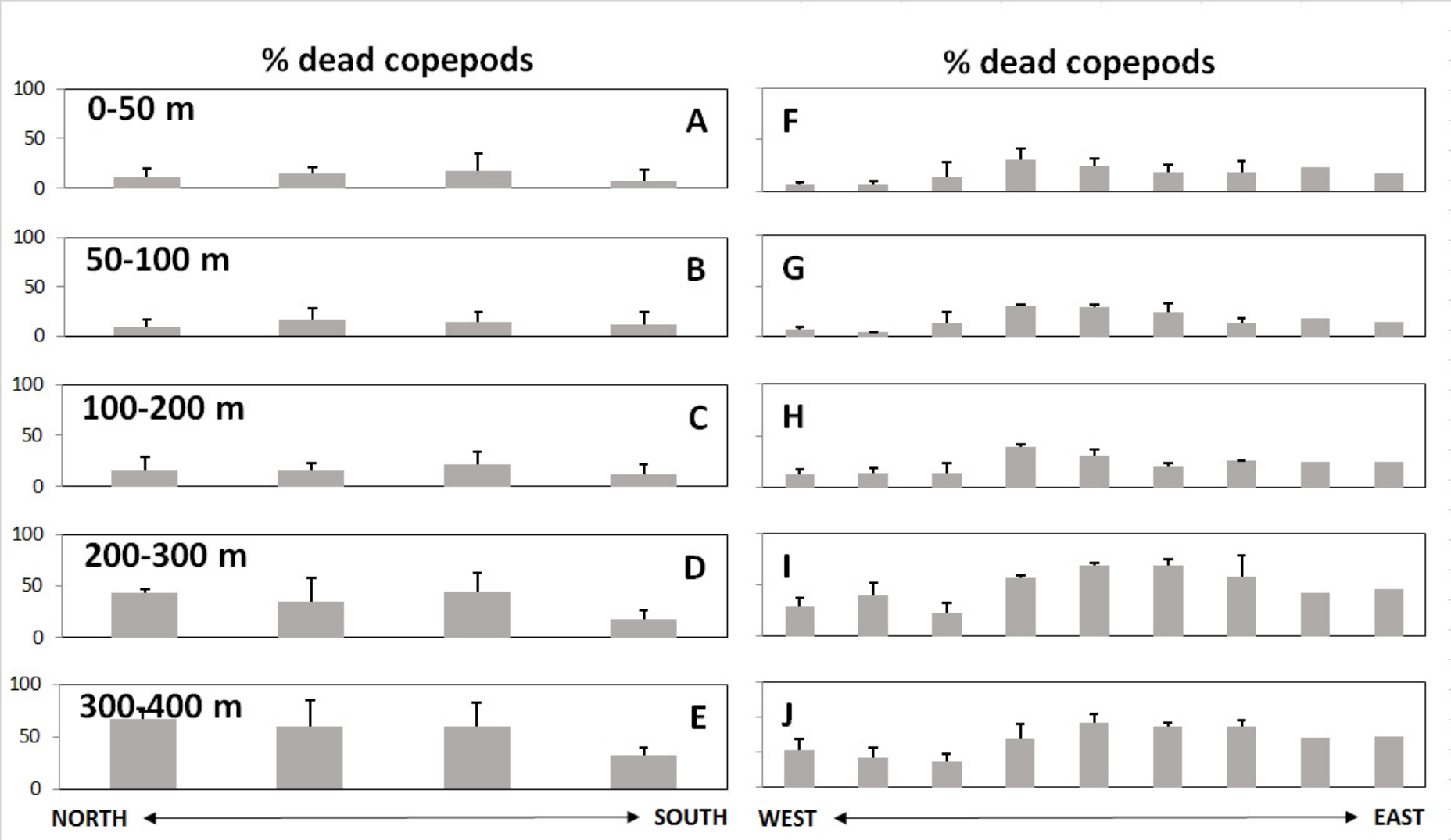
% dead copepods
% dead copepods
0-50 m
A
50-100 m
B
100-200 m
C
200-300 m
D
300-400 m
E
F
G
H
I
J
100
50
0
NORTH
SOUTH
WEST
EAST

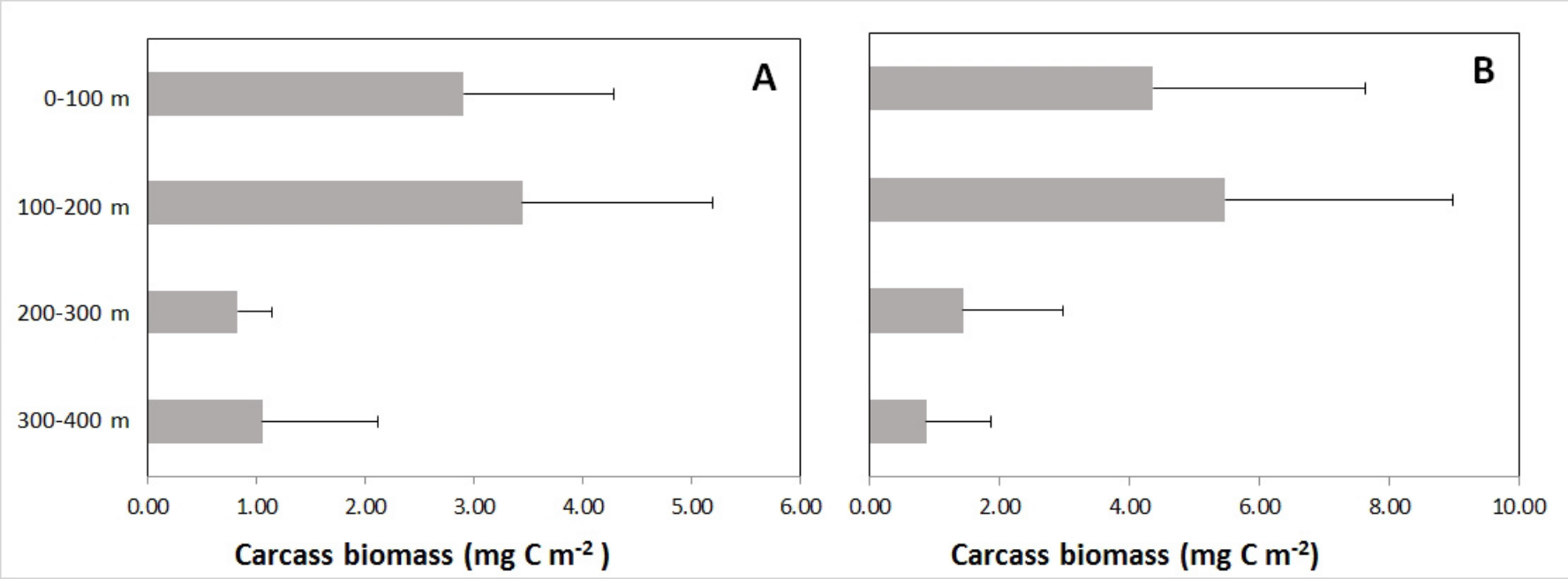
A
B
0-100 m
100-200 m
200-300 m
300-400 m
0.00
1.00
2.00
3.00
4.00
5.00
6.00
0.00
2.00
4.00
6.00
8.00
10.00
Carcass biomass (mg C m-2)
Carcass biomass (mg C m-2)

SUPPLEMENTARY MATERIALS

Table S1. SIMPER (similarity percentage) analysis showing the main operational taxonomic units (OTUs) explaining the dissimilarity between carcass-associated bacterial communities at 0 h and 24 h of the three carcass decomposition experiments.

Experiment 1 OTU closest relative	Average relative abundance (%) at t_0	Average relative abundance (%) at t_{24}	Contribution to dissimilarity (%)
Pseudomonadales	23.1	2.0	17.6
Rickettsiales	3.5	12.7	8.8
Pelagibacterales	2.4	7.1	5.8
Flavobacteriales	2.9	7.3	5.2
Thiotrichales	3.0	0.6	5.0
Oceanospirillales	7.7	13.2	4.5
Acidimicrobiales	0.7	2.7	4.0
Total	43.2	45.5	51.0
Experiment 2 OTU closest relative	Average relative abundance (%) at t_0	Average relative abundance (%) at t_{24}	Contribution to dissimilarity (%)
Vibrionales	16.8	36.3	10.6
Rickettsiales	11.0	3.1	8.5
Pseudomonadales	2.8	9.5	7.8
Oceanospirillales	12.6	4.9	7.3
Pelagibacterales	7.2	1.8	7.3
Acidimicrobiales	2.8	0.5	5.5
Synechococcales	2.6	0.5	4.8
Total	55.6	56.6	52.0
Experiment 3 OTU closest relative	Average relative abundance (%) at t_0	Average relative abundance (%) at t_{24}	Contribution to dissimilarity (%)
Vibrionales	20.6	46.3	22.4
Rickettsiales	11.2	2.2	18.3
Rhodobacterales	29.3	21.4	7.8
Pelagibacterales	2.7	1.0	6.1
Total	63.7	70.9	54.6

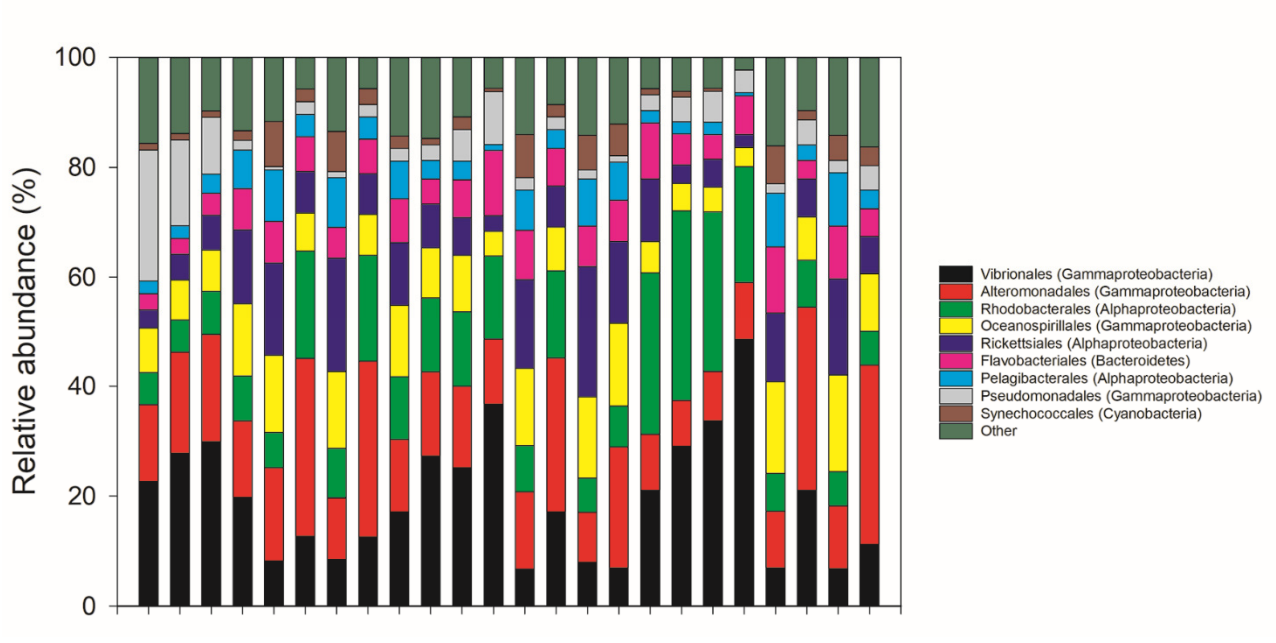

Fig. S1. Relative bacterial abundance (class) expressed as % of total sequences obtained in Exp. 1, 2 and 3 for "carcass" (triplicates), "carcass water" (five replicates) and "control water" (triplicates). "Other" includes taxa accounting for less than 0.3% of the relative abundance in a single sample. Bars represent sequence reads pooled from replicate samples.

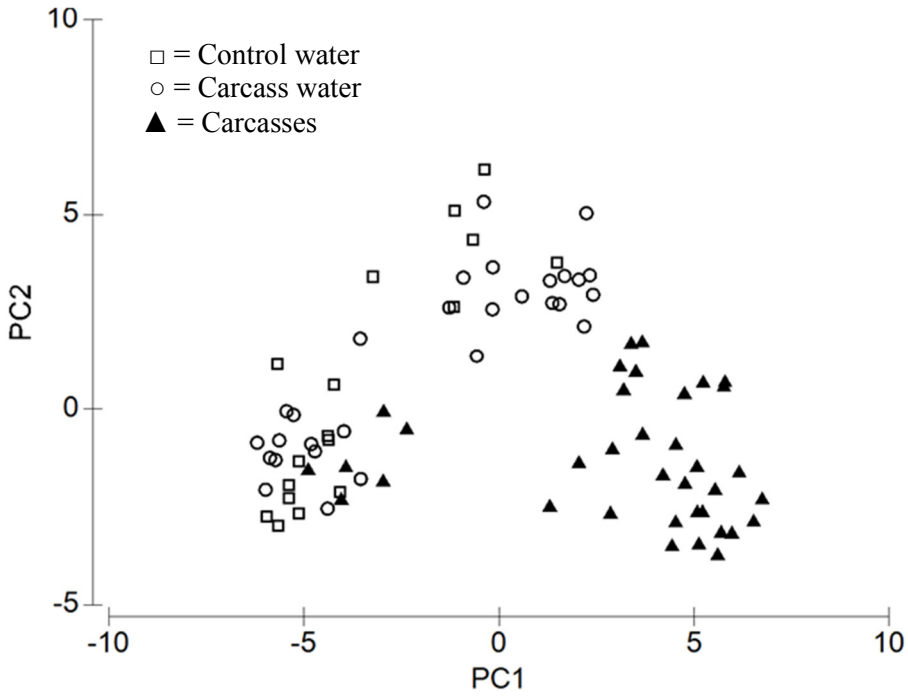

Fig. S2. Bacterial community composition and succession in carcass decomposition experiments. Principal coordinates comparison of carcass-associated (triangles) microbial community composition and those in carcass water (circles) and control water (squares), where PC1 and PC2 explain 52.1 and 18.5 % variations, respectively.